J Therm Anal Calorim (2011) 103:543–553
DOI 10.1007/s10973-010-0930-6

Response of a glass/phenolic composite to high temperatures

Michael L. Hobbs · James T. Nakos · Patrick D. Brady

Received: 23 April 2010 / Accepted: 11 June 2010 / Published online: 3 July 2010

Abstract Determining the response of composite phenolic materials to fire remains a major unsolved problem that is important for high consequence safety analysis. Difficulties arise when thermophysical property measurements are obscured by decomposition reactions. This article presents several decomposition experiments and models for a phenolic resin impregnated into chopped 1.27-by-1.27 cm glass fabric. The thermal response of the material was measured using thermogravimetric analysis (TG), differential scanning calorimetry (DSC), and laser flash diffusivity (LFD). The TG data was used to develop a 5-step decomposition mechanism describing mass loss due to reaction; the DSC data was used to describe the energy changes associated with these reactions; and the LFD data was used to describe energy flow into the decomposing material. An effective thermal conductivity model was used to partition energy transport by gas conduction, solid conduction, and diffusive radiation. The dynamic gas volume fraction is treated as a field variable to extrapolate thermal transport properties at high temperatures where decomposition is prevalent. These various models have been implemented into a finite element response model with an example calculation that includes uncertainty.

Keywords DSC · Effective thermal conductivity · Glass fabric · LFD · Model · Phenolic · TG · Uncertainty quantification

M. L. Hobbs (✉) · J. T. Nakos · P. D. Brady
Engineering Sciences Center, Sandia National Laboratories, Albuquerque, NM 87105, USA
e-mail: mlhobbs@sandia.gov

Introduction

Our laboratories' primary mission is to ensure that the U.S. nuclear arsenal is safe, secure, and reliable. Thermal insults such as fire are a major safety concern for these high consequence systems. Responses of interest include thermal energy transport and pressurization caused by decomposing organic materials such as polyurethane foams [1, 2], epoxy polymer encapsulants [3, 4], and glass fabric-filled phenolic composites [5]. Erickson [6] discusses various chemical decomposition mechanisms for many of these materials by examining decomposition products from TG using Fourier transform infrared spectroscopy.

Obtaining kinetic reaction rates for these proposed mechanisms is a challenge as discussed by Chrissafis [7]. Chrissafis recently reviewed the advantages and disadvantages of using single or multiple heating rate data as well as using single or multiple step reactions when describing polymer decomposition. Chrissafis concluded that one should use multiple heating rates for more reliable kinetic evaluations and that multiple reaction steps give better results.

We agree with Chrissafis conclusions and add that run-to-run variability should also be taken into account. Slight disagreement between model predictions and measurements at different heating rates can be explained by experimental as well as model uncertainty. Uncertainties in model predictions arise from uncertainty associated with input parameters. Uncertainty is accounted for in the current study using smart sampling techniques such as Latin Hypercube Sampling (LHS) [8].

Measurements of thermal physical properties at elevated temperature are confounded when materials decompose. Unsolved challenges at these high temperatures include measuring thermal conductivity and specific heat during

decomposition. Difficulties arise when the endothermic and/or exothermic reaction enthalpies confound the thermophysical property measurement. Significant volume changes as well as vitrification in some of these materials complicate the measurements.

We postulate that changes in thermophysical properties at elevated temperatures correlate with the gas volume fraction similar to effective thermal conductivity models discussed in [9] and [10]. Thermal expansion of the polymer matrix causes the gas volume fraction to decrease to accommodate the change in the polymer volume. In contrast, gas volume fraction increases as the polymer matrix is converted into decomposition gases. We hypothesize that conduction through the decomposing materials depend on the evolving gas volume fraction. In the current article, our modeling and experimental methods are applied to MXB-71 [5], a glass fabric-filled phenolic composite made using a phenolic resin impregnated into chopped 1.27-by-1.27 cm glass fabric.

MXB-71 experiments

A TA Instruments Model Q5000 TGA was used to obtain changes in mass as the temperature of a 4.9 mg sample was increased at 20 °C min^{-1} as shown in Fig. 1a. Figure 1a shows the remaining solid mass (m) normalized by the initial sample mass (m_0), $S_f = m/m_0$. S_f is the reacted solid mass fraction. The derivative of the TG mass loss curve, also shown in Fig. 1a, can be used to identify the temperature where weight loss is most apparent. The heat flow necessary to increase the temperature of a 13.5 mg sample at 20 °C min^{-1} is shown in Fig. 1b. The heat flow was measured with a TA Instruments Model DSC 2920. Large decreases and increases in heat flow correlates with weight loss shown by the TG data. Since TG and DSC techniques are commonly used, they are not described in detail in this article.

The laser flash diffusivity (LFD) device was used to measure the thermal conductivity by exposing a 1.27 cm diameter by 1–2 mm thick sample to a "flash" laser light on one of the flat sample surfaces. The heat conducts through the sample to the other side where temperature is measured. A simple one-dimensional heat diffusion equation is used to reduce the data to estimate the thermal diffusivity [11]. The average value of the thermal conductivity was 0.46 W m^{-1} $°C^{-1}$ (20–200 °C) with an uncertainty of about 5%.

Various MXB-71 samples were placed in an oven with an Argon purge for 30 min to cure the sample for the LFD measurement at temperatures higher than 200 °C. The purpose for curing the samples was to eliminate decomposition products so that the thermal conductivity of the

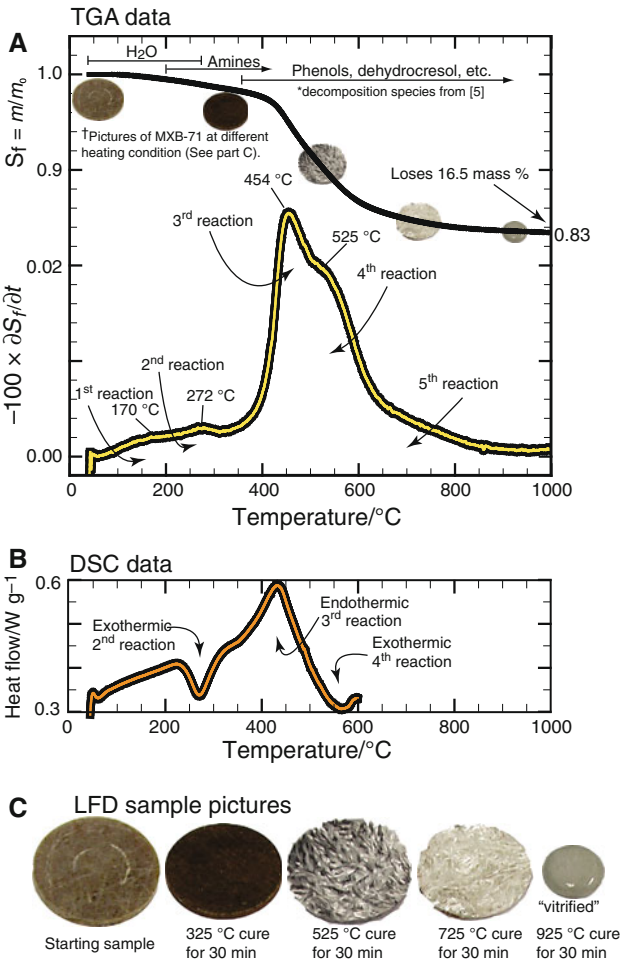

Fig. 1 **a** TG mass loss history, **b** DSC heat flow, **c** pictures of cured LFD samples

degraded MXB-71 could be measured at high temperatures without interference from decomposition chemistry. At 325 °C, the sample darkened but had a similar shape to the starting sample. At 525 °C, most of the phenolic resin decomposed and randomly oriented glass fibers were discernable. At 725 °C, all of the phenolic resin had decomposed leaving light colored glass fibers. The cured sample at 725 °C was warped and fragile. At 925 °C, the LFD sample vitrified.

Pictures of cured LFD samples are shown on the mass loss curve at the corresponding cure temperatures and also in Fig. 1c. Significant volume changes and likely enthalpy changes occur above 725 °C, which were not measured by the DSC experiment. Only ambient pressure results are addressed in the current article. The effects of pressure and confinement on decomposition are beyond the scope of the current study, but should be considered in the future.

Because of the inability to eliminate chemistry effects at elevated temperatures, we have modeled the thermal conductivity above 200 °C by separating conductive heat

transfer into three parts: conduction through the solid, conduction through the decomposition gases, and diffusive radiation. The relative contributions depend on the gas volume fraction, which is determined as a field variable. The following sections describe the decomposition model with comparison to data. Subsequent sections describe a response model for MXB-71 including contributions due to gas conduction, condensed conduction, and diffuse radiation.

MXB-71 decomposition model

The derivative of the reacted solid mass fraction in Fig. 1a indicates that four reactions centered about 170, 272, 454, and 525 °C describe decomposition. A fifth reaction with the center obscured by the 3rd and 4th reactions could be used to describe the slope change at 650 °C. Table 1 gives a five-step decomposition model with parameters that can accurately describe the mass loss in Fig. 1a. The DSC data in Fig. 1b suggests the first reaction is thermally neutral, the 2nd reaction is exothermic, the 3rd reaction is endothermic, the 4th reaction is exothermic, and the reaction enthalpy of the 5th reaction is uncertain. The 5th reaction is assumed to be thermally neutral although endothermic processes associated with vitrification are expected. More data beyond 600 °C is needed to establish these enthalpy changes.

Five reaction rates were distributed normally with respect to the extent of reaction to approximate the effect of thermal damage. This method of describing reaction rates is different from traditional methods described by Chrissafis [7] in that portions of the material are assumed to evolve at different first-order rates. Distributing activation energies smoothes the reaction rates and eliminates abrupt changes in calculated solid fractions in agreement with observations. Pitt [12] first used distributed activation energies with a single reaction to approximate decomposition of coal as a many component mixture that decomposed independently. The normally distributed reaction rates for the first-order reaction steps given in Table 1 are:

$$\frac{\partial C_i}{\partial t} = \xi_i A_i \exp\left(\frac{-E_i + z\sigma_i}{RT}\right) C_i \quad \text{with}$$

$$1 - \frac{C_i}{C_{o,i}} = \int_{-\infty}^{z_i} \frac{1}{\sqrt{2\pi}} \exp\left(\frac{-z_i^2}{2}\right) \mathrm{d}z_i \quad \text{or}$$

$$z_i = normsinv\left(1 - \frac{C_i}{C_{o,i}}\right), \tag{1}$$

where i represents the ith reaction and ranges from 1 to 5. "z" is the ordinate of the standard normal cumulative distribution function representing the number of standard deviations above or below the mean activation energy. In Eq. 1, the quantity, $1 - C_i/C_{o,i}$, represents the progress of the ith reaction. The function *normsinv* returns the inverse

Table 1 Five step decomposition model with parameters

Symbol	Description	Units	Reactions: $C_i \rightarrow G_i$, $i = 1, 5$				
			1	2	3	4	5
C_o	Initial concentration	Mass fraction	0.010 ± 5%	0.002 ± 5%	0.023 ± 5%	0.065 ± 5%	0.066 ± 5%
E/R	Normalized activation energy	K	20,000	23,000	29,000	30,000	34,000
σ/R	Dispersion in activation energy	K	2,000	200	300	1,500	5,500
Ln (A)	Natural logarithm of prefactors	Ln (s^{-1})	37.0	37.0	35.7	32.8	33.7
h	Reaction enthalpies	kJ g^{-1} (cal g^{-1})	0	6.28 (1,500) ± 5%	−1.67 (−400) ± 5%	1.38 (330) ± 5%	0
ξ	Reaction rate uncertainty[a]	None	1 ± 20%	1 ± 20%	1 ± 20%	1 ± 20%	1 ± 20%

i represents species and reactions (1) through (5)

[a] The reaction rate uncertainty is 1 ± 20% implemented as a rate multiplier

of the standard normal cumulative distribution function. Essential parameters, descriptions with units, and uncertainty for this reaction mechanism are in Table 1. The solid mass fraction is $S_f = 1 - \sum G_i$ where $G_i = C_{o,i} - C_i$. Reverse reactions, which may be important for confined decomposition, were not included in the kinetic mechanism.

Mean predictions of the TG and DSC experiments

Figure 2 shows predictions of the TG mass loss data and the DSC heat flow data discussed previously with Fig. 1. The mean parameters from Table 1 were used for the simulations in Fig. 1. The heating rate for the TG experiment was 20 °C min^{-1} ($T = 0.3336t + 311.97$). The heating rate for the DSC experiment was slightly higher at 20.2 °C min^{-1} ($T = 0.3372t + 306.66$). The five step mechanism with the mean input parameters given in Table 1 were used to fit the data. The lines labeled 1–5 represent the mass loss and derivative of mass loss associated with each of the five *independent* reactions. The individual reacted mass loss fractions were determined by $S_{f,i} = 1 - G_i$. The sum of the individual reacted solid fractions is given by the solid black line, which is in agreement with the data represented by circles.

The derivative of the mass loss shows that the first and last reactions are broad and do not show prominent peaks in the derivative curve, especially the last reaction. In contrast the 2nd, 3rd, and 4th reactions are narrower with distinct peaks. The second reaction does not contribute significantly to the mass loss, but was included to capture the first exothermic reaction in Fig. 2b. The heat flow indicates that this reaction occurs over a small temperature range that is probably a curing agent burning off. Both the 1st and 5th reactions were assumed to have a net enthalpy change of zero. Heat flow was calculated in Fig. 2b as the sum of the sensible and reaction energy, $q_{\text{flow}} = q_{\text{sen}} + q_{\text{rxn}}$ where $q_{\text{sen}} = C_p \frac{\partial T}{\partial t}$ and $q_{\text{rxn}} = \sum_i r_i h_i$ with $r_i = \xi_i A_i \exp[(-E_i + z\sigma_i)/\text{RT}] C_i$.

Figure 2b shows the overall reaction enthalpy determined as the difference between the integral of the sensible energy and the heat flow as $h_{\text{rxn}} = \int q_{\text{flow}} \text{d}t - \int q_{\text{sen}} \text{d}t = \int q_{\text{rxn}} \text{d}t = 64 \text{ J g}^{-1}$. The sensible energy is depicted in Fig. 2b as a dashed purple line. The energy release associated with decomposition of MXB-71 phenolic is small when compared to more energetic materials such as TNT which has an overall reaction enthalpy of 5,400 J g^{-1} [13].

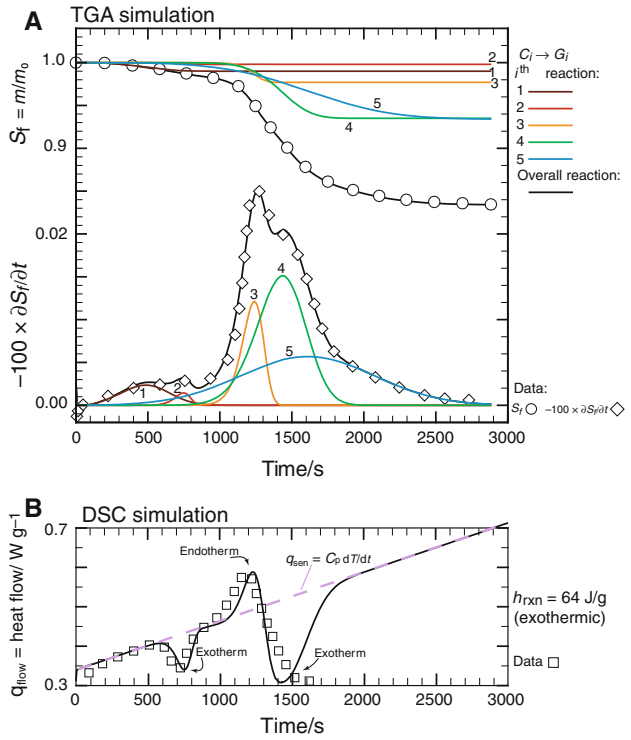

Fig. 2 Predicted (*lines*) and measured (*symbols*), **a** TG mass loss history at 20 °C/min and **b** DSC heat flow (*solid black line*) with sensible energy (*dashed purple line*) history at 20.2 °C/min

Uncertainty predictions of the TG and DSC experiments

Uncertainties in the calculated results for the TG simulations were determined using a Latin hypercube sampling (LHS) technique. The LHS technique is an efficient, *constrained sampling* technique developed by McKay et al. [8] to propagate uncertainty into the predicted results. Thirteen of the parameters listed in Table 1 show uncertainty. A five percent uncertainty was associated with the initial concentrations; a 5% uncertainty was associated with the reaction enthalpies for reactions 2, 3, and 4; and a 20% uncertainty was associated with the five reaction rates. All of the uncertainty intervals were assumed to be uniformly distributed. The uncertainty intervals were arbitrarily chosen to show the impact of parameter uncertainty. A detailed experimental program is needed to determine the actual uncertainty with its associated distribution.

The reaction uncertainty was implemented as a simple rate multiplier to avoid interaction between activation energy, dispersion, and frequency factor. Since there is correlation between the activation energy, dispersion, and prefactor, one would expect many combinations of these variable to give similar results, especially when one considers uncertainty. This effect has been described by Brill et al. [14] as a kinetic compensation effect. A simple rate multiplier allows one to look at the uncertainty in the reaction rate without being confounded by kinetic compensation.

The effect of parameter uncertainty was accounted for by selecting 14 different values for each of the 13 parameters. The range of each input parameter was divided into

14 non-overlapping intervals based on equal probability. One random value from each interval was selected according to the probability density function in the interval. The 14 values thus obtained from the first parameter were then paired in a random manner with the 14 values obtained for the second parameter. These 14 pairs were then combined in a random manner with the 14 values of third parameter to form 14 triplets, and so on, until 14 sets of the 13 input variables were formed. The TG mass loss was then calculated 14 times with the 14 different sets of input parameters. The mean and standard deviation of the TG mass loss was then calculated from the 14 set of responses. The mean and standard deviation of the mass loss derivative was calculated in an analogous manner.

Figure 3a shows the uncertainty in the TG simulations. Figure 3b shows which parameters contribute the most to prediction uncertainty. The solid black line represents the mean predictions from 14 Latin Hypercube Simulations (LHS). The dashed lines represent the 95% prediction interval determined using a Student's *t*-distribution with 13 df ($\mu \pm 2.16\sigma$). The parameters which contribute the most to the uncertainty are determined by calculating importance factors. Importance factors provide the fraction of the uncertainty that is attributed to a given parameter and sum to unity. The importance is calculated by assuming that the response (mass loss or derivative of mass loss) is linear with respect to each input parameter. Linear regression is used to determine sensitivity coefficients, which are used with a mean value analysis [15] to determine importance.

Only 14 LHS runs ($n + 1$ with n being the number of model parameters) are required to determine the importance of the 13 input parameters using the mean value method. This method is computationally efficient for intense uncertainty analysis where one seeks a minimum number of LHS runs. For example, a minimum number of LHS runs is desired when one computes the uncertainty in a response variable that changes in time, such as the uncertainty of the mass loss or heat flow associated with the TG and DSC. With more LHS runs, one can relax the linear response assumption. Instead, scatter plots can be used to visually determine correlation between model parameters and model response. Toward the end of this article, a more complete LHS sensitivity model is used to explore the sensitivity of the response model. For this analysis, scatter plots of the response indicates that the variable that contribute to uncertainty are indeed linear, validating the linear assumption used in the mean value approach for the TG and DSC analysis.

As shown in Fig. 3a, the uncertainty in the mass loss is less than 1% at 3,000 s when the sample temperature is 1,000 °C. Most of the uncertainty in the mass loss prediction occurs after 1,500 s. The primary parameters that contribute

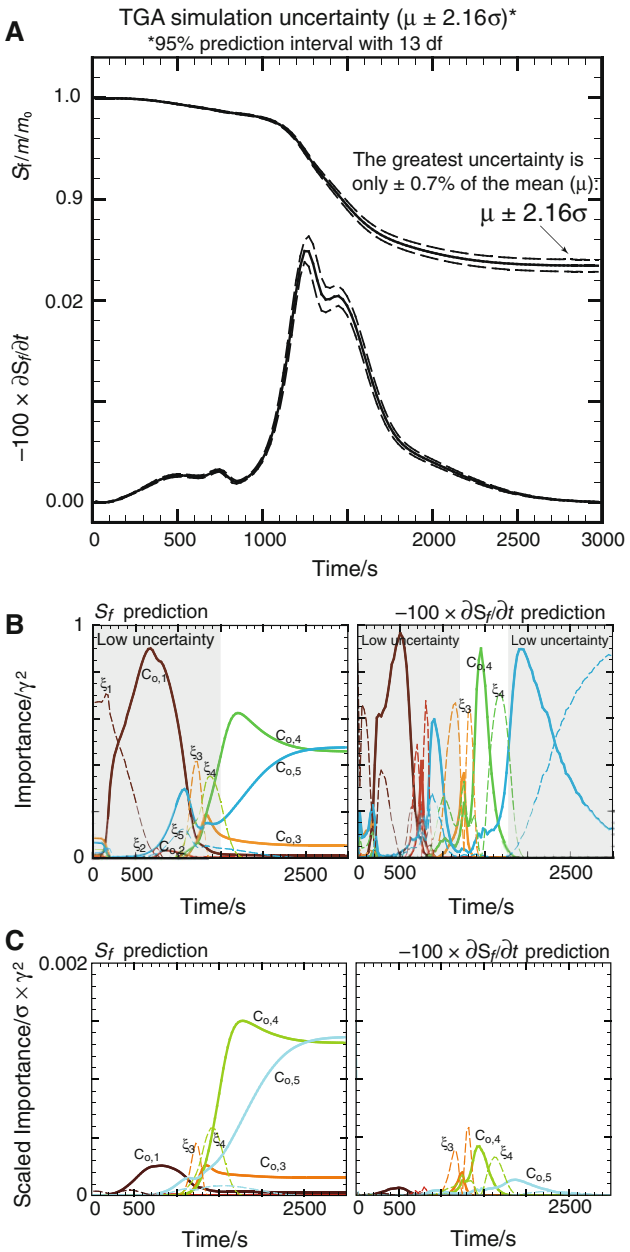

Fig. 3 **a** Uncertainty in TG predictions, **b** importance, **c** scaled importance

to the mass loss uncertainty are the initial concentrations used in the 3rd, 4th, and 5th reactions, as shown in Fig. 3b. In Fig. 3b, the areas of low uncertainty are shaded gray. Figure 3c shows the importance scaled by the standard deviation of the response. The scaled uncertainty clearly shows the sensitivity of the results to the initial concentrations. The uncertainty associated with the derivative of the mass loss predictions are given on the right-hand-side of Fig. 3b. In the derivative prediction, most of the uncertainty is between 1,000 and 2,000 s. The parameters that influence the uncertainty in this range are the initial concentrations

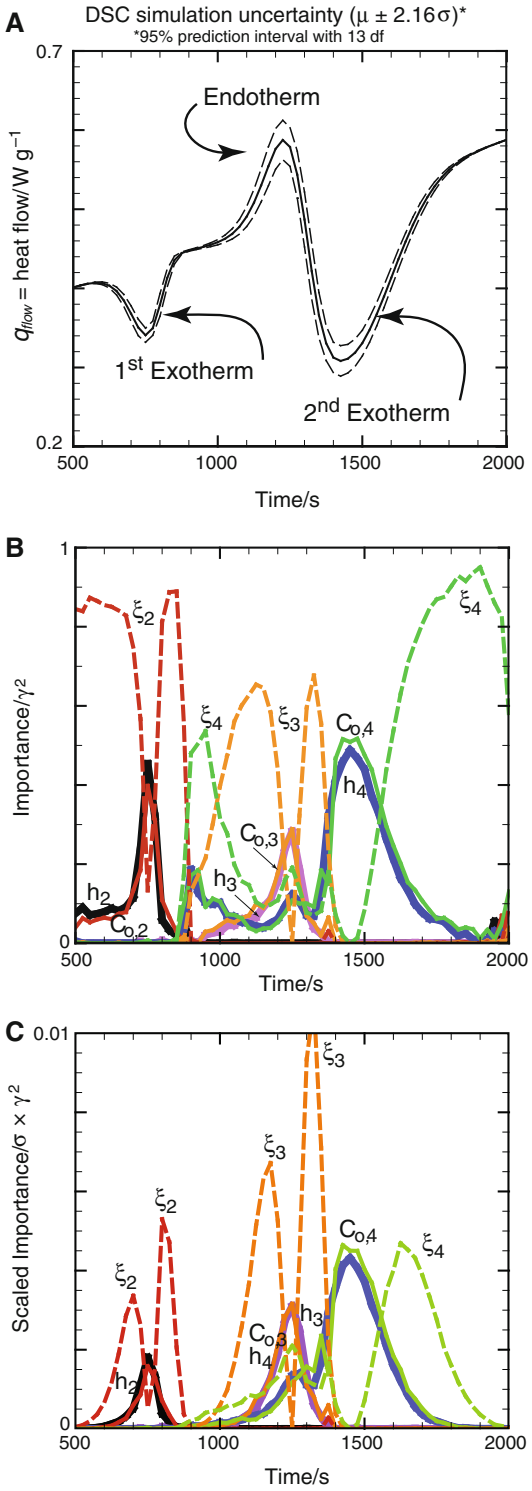

Fig. 4 **a** Uncertainty in DSC predictions, **b** importance, **c** scaled importance

used in the 4th reaction and the reaction rates of the 3rd and 4th reactions. Note that the uncertainties in the reaction enthalpies do not affect the mass loss predictions since the temperature of the sample is specified.

Figure 4a shows the uncertainties associated with the prediction of the heat flow in the DSC experiment. Figure 4b, c shows which parameters contribute the most to the prediction uncertainty. As in the TG prediction, the solid black line represents the mean from 14 Latin Hypercube Simulations (LHS). The dashed lines bound the 95% prediction interval determined using a Student's *t*-distribution with 13 df ($\mu \pm 2.16\sigma$). The parameters that contribute to the uncertainty of the first exotherm are related to the 2nd reaction. Likewise, the parameters associated with the endotherm are related to the 3rd reaction, and the parameters responsible for the final exotherm are related to the 4th reaction. Parameters associated with reactions (1) and (5) do not affect the heat flow prediction. The importances of the reaction enthalpies are the same as the initial concentrations since the uncertainty in these parameters were the same (5% of the mean).

MXB-71 response model

The response of the MXB-71 was determined with a finite element model that solves the heat diffusion equation with a source term for chemistry,

$$\rho C \frac{\partial T}{\partial t} = \nabla \cdot (k_{\text{eff}} \nabla T) + \sum_{i=1}^{5} q_i r_i, \tag{2}$$

where ρ, C, T, t, k_{eff}, q, and r represent material density, specific heat, temperature, time, effective thermal conductivity, volumetric reaction energy, and reaction rate, respectively. The reaction rates were discussed previously with $r_i = \frac{\partial C_i}{\partial t}$. Enclosure or surface-to-surface radiation can be calculated by solving the following radiation enclosure equation:

$$\sum_{j=1}^{N} \left[\frac{\delta_{kj}}{\varepsilon_j} - F_{k-j} \left(\frac{1-\varepsilon_j}{\varepsilon_j} \right) \right] \frac{Q_j}{A} = \sum_{j=1}^{N} \left(\delta_{kj} - F_{k-j} \right) s T_j^4. \tag{3}$$

Q represents the energy transfer between surfaces in an enclosure where δ_{kj} is the unit tensor, s is the Stefan-Boltzmann constant, ε is the emissivity, and F_{k-j} is the radiation view factor defined as the fraction of energy leaving surface j and arriving at surface k.

Solution of Eqs. 2 and 3 gives the time-resolved temperature and species concentrations within the phenolic and the temperature in the inert materials such as the confining metal skin and embedded components. In this article, the boundary temperatures of the high-conductivity confining hardware are specified. The thermophysical properties such as specific heat are based on measurements. The emissivity of the phenolic was taken to be 0.8 since materials with rough surfaces typically have emissivities that approach unity. Initial bulk density was assumed to be 1,800 kg/m^3 based on measurements.

The thermal conductivity of the phenolic is partitioned into three contributions: conduction through the condensed phenolic, λ_c; conduction through the gas, λ_g; and radiation through the cell walls and across the cell voids, λ_r:

$$k_{\text{eff}} = \lambda_c + \lambda_g + \lambda_r, \quad \text{with} \quad \lambda_c = \frac{2}{3}(1-\phi)k_c,\ \lambda_g = \phi k_g$$
$$\text{and} \quad \lambda_r = \frac{16sT^3}{3\left[\phi\alpha_g + (1-\phi)\alpha_c\right]}. \tag{4}$$

In Eq. 4, ϕ is the gas volume fraction, $\phi = 1 - \frac{S_f\rho_c^o(1-\phi^o)}{\rho_c}$; k_c is the thermal conductivity of the condensed phenolic, and k_g is the thermal conductivity of the gas within the voids. The contributions due to gas-phase conduction (λ_g), condensed-phase conduction (λ_c), and radiation (λ_r) at room temperature are 0.0003, 0.46, and 0.0002 W m^{-1}K^{-1}, respectively, for an effective thermal conductivity of 0.46 W m^{-1}K^{-1} as measured by LFD discussed previously. Other quantities of interest include the initial gas volume fraction (ϕ^o), the condensed density (ρ_c), the gas density (ρ_g), and the bulk density (ρ_b) which are $\phi^o = \frac{\rho_c^o - \rho_b^o}{\rho_c^o - \rho_g^o} \approx 1 - \frac{\rho_b^o}{\rho_c^o}$, $\rho_c = \rho_c^o/[1+\beta(T-T^o)]$, $\rho_g = \frac{PM_w}{RT}$, and $\rho_b = \phi\rho_g + (1-\phi)\rho_c$, respectively. For open systems, the pressure (P) is a constant. For closed systems, pressure can be calculated using a low Mach flow assumption wherein $\nabla \cdot P = 0$. In other words, pressure is assumed to be spatially constant, but varies in time due to temperature changes and reaction.

In Eq. 4, $\frac{2}{3}$ represents a tortuosity correction [16]. For example, only four of the six sides of a hollow cube contributes to conduction, or $\frac{4}{6} = \frac{2}{3}$. The thermal conductivity of the gas is assumed to be the same as the conductivity of CO_2 varying linearly in temperature with k_g at 300 and 500 K being 0.0166 and 0.0325 W m^{-1} K^{-1} [17], respectively. The gas volume fraction, ϕ, is a function of the reacted solid fraction and the density of the condensed phase, ρ_c. The condensed phase density changes with temperature as the phenolic thermally expands with β being the volumetric thermal expansion coefficient assumed to be 135×10^{-6} K^{-1} based on the volume change of phenolic materials [18]. α_g and α_c are the absorptivity of the gas and polymer with value of 100 and 50,000 m^{-1}, respectively. The gas absorptivity is based on air and the condensed absorptivity is based on polyurethane. These values have been used to describe explosive decomposition [13, 19] and are considered representative values. The response model is not sensitive to the absorptivity since the radiation contribution to energy transport is small. The initial gas molecular weight in the pores was assumed to be 44 g mol^{-1}. The decomposition gas molecular weight was assumed to be 150 g mol^{-1}.

Figure 5a shows the effective thermal conductivity with contributions due to gas conduction, condensed-phase conduction, and diffuse radiation. The condensed conduction dominates since the gas volume fraction is relatively small. Figure 5b shows that the gas conduction (λ_g) is proportional to the gas volume fraction (ϕ). Initially, the condensed phenolic thermally expands making the gas volume fraction decrease. As the solid fraction (S_f) decreases, gas accumulation causes the gas volume fraction (ϕ) to increase.

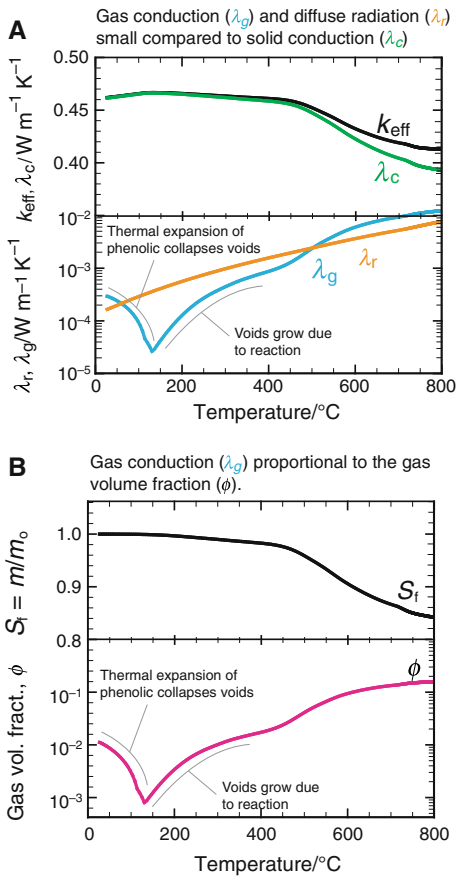

Fig. 5 **a** Effective thermal conductivity with contributions due to gas conduction, condensed-phase conduction, and diffuse radiation, **b** reacted solid fraction and gas volume fraction

The effective thermal conductivity model uses a diffusion approximation for the optically thick medium [20]. The diffusion approximation requires that intensity in the foam be nearly isotropic, which is a good assumption in the bulk of the phenolic. However, the approximation is not valid near certain types of boundaries, i.e., shiny boundaries with low emissivities. However, the boundaries in applications where organic materials are decomposing are probably not shiny but are likely to have emissivities near unity. Thus, the diffusion approximation is probably acceptable near these types of boundaries. "Radiation slip" or "jump" boundary conditions need to be applied to boundaries that have large anisotropies [20]. "Radiation slip" is beyond the scope of the current study.

Table 2 Additional parameters for response model

Parameter	Description	Values
α_c, m^{-1}	Condensed absorption coefficient	50,000 ± 10%
α_g, m^{-1}	Gas absorption coefficient	100 ± 10%
$C_{p,0\ °C}$, J kg^{-1} K^{-1}	Heat capacity[a] at 0 °C	937 ± 10%
$C_{p,50\ °C}$, J kg^{-1} K^{-1}	Heat capacity[a] at 50 °C	1,025 ± 10%
$C_{p,230\ °C}$, J kg^{-1} K^{-1}	Heat capacity[a] at 230 °C	1,221 ± 10%
k_c, W m^{-1} K^{-1}	Condensed thermal conductivity	0.7 ± 10%
ρ_{bo}, kg m^{-3}	Initial bulk density (guessed)	1,780 ± 5%
ρ_{co}, kg m^{-3}	Initial condensed phase density	1,800 ± 5%

[a] Heat capacity is linearly interpolated. For $T > 230$ °C, $C_p = C_{p,230\ °C}$

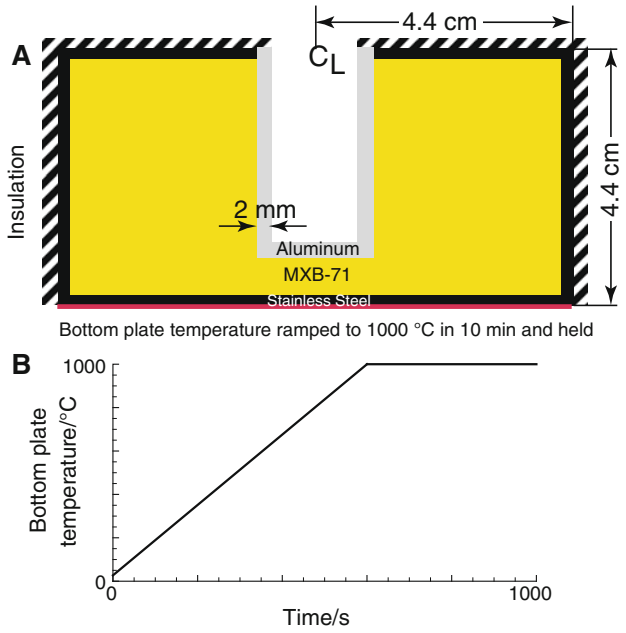

Fig. 6 **a** Schematic of geometry for example calculation and **b** bottom plate temperature. All external surfaces except the bottom plate were assumed to be insulated

Response model with uncertainty

A sample calculation with uncertainty was performed to demonstrate the response of MXB-71 to abnormal thermal environments. The same chemistry parameters including uncertainty were used for the response calculations. Additional parameters for the response model including uncertainty are listed in Table 2. Figure 6a shows the configuration where the phenolic is depicted as an 8.4-cm diameter, 4-cm high cylinder with a 2-cm diameter, and 3.6-cm high hollow aluminum cylinder embedded in the center. The distance from the stainless steel/MXB-71 interface to the aluminum/MXB-71 interface is 0.6-cm.

The confining stainless steel is an 8.8-cm diameter and 4.4-cm high cylinder. The wall thickness of the stainless steel and aluminum are 2-mm. All surfaces were assumed to be insulated except for the bottom plate which was heated from room temperature 27 °C to 1,000 °C in 10 min as shown in Fig. 6b. The total simulation time was 1,000 s.

Both 3D and 2D axisymmetric meshes are shown in Fig. 7. Under each mesh, the solution at 1,000 s is shown using the mean parameters in Tables 1 and 2. Half of the 3D solution is removed for comparison to the 2D solution. Figure 7a shows the 2D solution with contours representing the gas volume fraction from 0.165 to 0.0017. The contours in the 3D solution in Fig. 7b represents the reacted solid fractions from 0.83 to 0.98. Both solutions have seven temperature isotherms ranging from 400 to 1,000 °C. The 2D and 3D solutions give quantitatively similar results.

The time required for the bottom of the hollow aluminum cylinder to reach 500 K (227 °C) was used as a response metric to determine the sensitivity of the uncertain parameters in Tables 1 and 2. This response metric was arbitrarily chosen to demonstrate the sensitivity of the response model. In real applications, the response temperature might represent the failure temperature of an embedded component and the distance of 0.6-mm from the heated surface may represent the distance to an abnormal thermal boundary such as an accidental fire. However, in the current study, the selection of 500 K and a distance of only 6-mm from the heated boundary are only examples. The sensitivity for other response temperatures and distances from the heated boundary will undoubtedly result in different sensitivities.

An LHS analysis with 100 samples was used to determine the sensitivity of the component response time. The mean and standard deviation of the 100 LHS samples is given in the histogram plotted in Fig. 8. The mean time to reach 500 K was 603 s with a standard deviation of 16 s. The distribution of each uncertain input parameter was assumed to be uniform. The histogram indicates that the component response time is normally distributed with respect to the uncertainty in the input parameters.

To measure the correlation strength or *sensitivity* of the response time, the standard linear correlation coefficient was computed for each of the uncertain input parameters given in Fig. 8:

$$r = \frac{\frac{1}{n-1}\sum_{i=1}^{n}(t_i - \mu_t)(y_i - \mu_y)}{\sigma_t \times \sigma_y}, \quad (5)$$

where μ_t represents the mean or average computed response time in the $n = 100$ LHS runs; μ_y is the mean of the 100 corresponding LHS input values for the uncertain

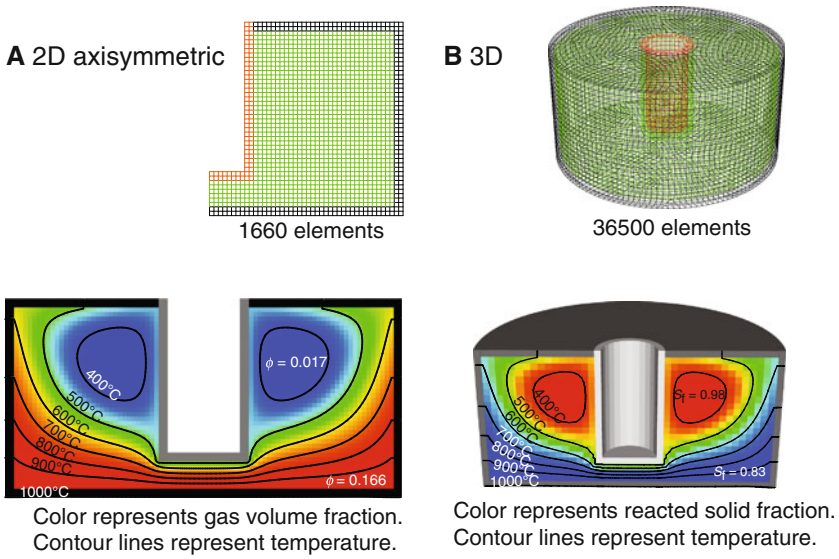

Fig. 7 Mesh and solution for **a** 2D axisymmetric and **b** 3D simulations

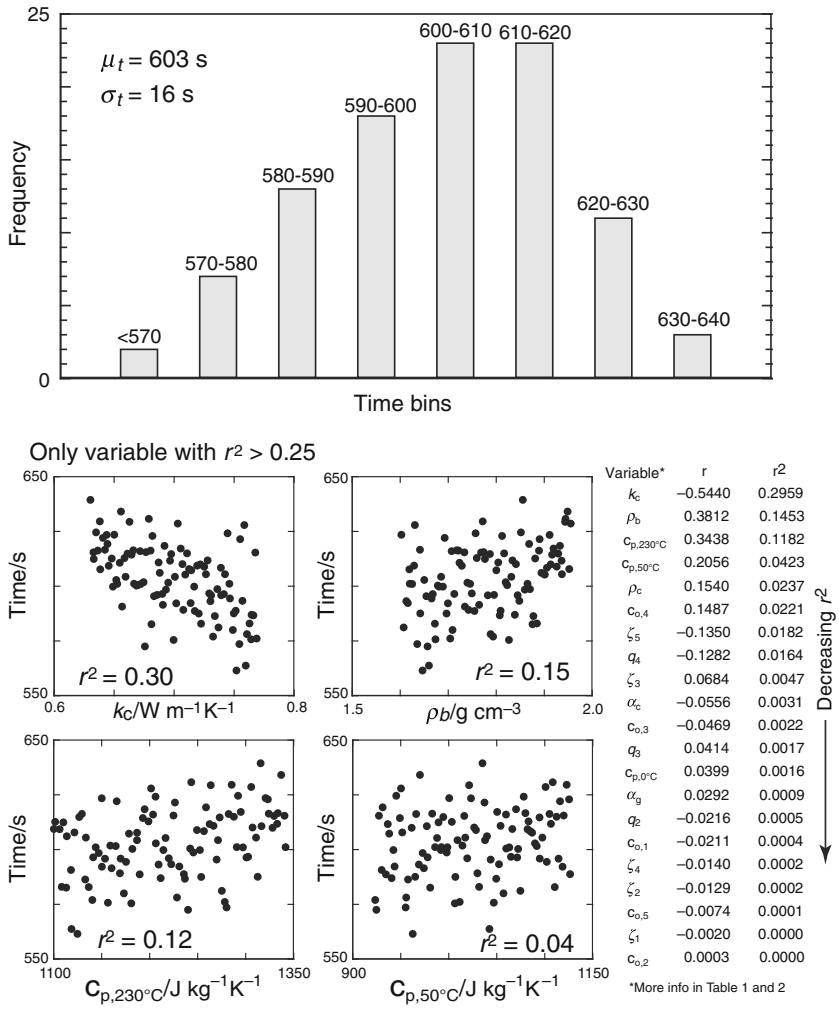

Fig. 8 Histogram (*top*) of 100 LHS calculated component responses and scatter plots (*bottom*) of the four parameters with the highest r^2 values

variable y; σ_t and σ_y are the standard deviations of the response time and input values.

A perfect positive or negative linear correlation is $|r| = 1$. In the current article, the linear correlation strength is considered significant when $|r| > 0.5$ or $r^2 > 0.25$. Such judgments of r values *depend* on whether a linear model is a good fit of the simulation results. Examination of *scatter* plots of response versus parameter values is a better way to

judge any strongly organized linear or nonlinear relationship between the model parameters and the model response. Scatter plots of the parameters with the four highest r^2 values are plotted on the bottom of Fig. 8. The condensed conductivity is weakly correlated and shows a decreasing trend. As the condensed conductivity increases, heat can penetrate the material faster and time for the embedded component to reach 500 K decreases. Correlation with the other three variables gets progressively weaker. Scatter plots for the other variables show similar behavior.

Summary and conclusions

Accurate prediction of the response of complex systems containing organic materials exposed to abnormal thermal environments such as fire is a complex and complicated problem. Difficulties arise when thermal physical properties are measured at temperatures above decomposition thresholds. Transport property measurements such as thermal conductivity and specific heat are confounded by energy and volume changes caused by reactions. As an example of such problems, we have measured the response of a glass/phenolic material (MXB-71) exposed to high temperatures. We have attempted to make transport property measurements at elevated temperatures by curing samples in an oven. The problem with such methods is that the material continues to decompose after being cured. And at temperatures near 925 °C the material vitrified. In order to predict material response at these high temperatures, we have modeled the decomposition and evolution of the gas volume as field variables. The thermal conductivity was then partitioned into contributions due to gas conduction, condensed conduction, and diffusive radiation. The predictions were most sensitive to the condensed thermal conductivity.

A five-step mass loss model with distributed activation energies was used to predict the mass loss of MXB-71 phenolic exposed to fire-like heat fluxes using an effective thermal conductivity model. The activation energies, pre-exponential factors, and distribution parameters were obtained from TG experiments. Reaction enthalpies and specific heats were obtained from DSC data. Low temperature thermal conductivities were obtained from LFD data. The measured specific heat was assumed to be a linear function of temperature between 50 °C and 230 °C. For temperatures greater than 230 °C, the specific heat capacities were assumed to be constant. The model was used to predict mass loss from a TG experiment with a 20 °C/min ramp and also to predict energy changes associated with the DSC experiment. Uncertainty in the prediction was determined with LHS analysis. The 95% prediction interval was less than 1 percent of the mean indicating that the chemistry model was adequate to determine mass loss. The simulation of the DSC energy changes was similar. However, enthalpy changes above 600 °C are uncertain since DSC data above this temperature were not obtained.

The MXB-71 constitutive model was implemented into a finite element code and used to predict the response of an 8.4-cm diameter by 4-cm high right circular cylinder with a 2-cm diameter hollow aluminum cylinder embedded in the center. A 2-mm thick stainless steel confining skin enclosed the phenolic. The bottom of the confinement was ramped from room temperature to 1,000 °C in 10 min and held. This geometry and heating rate were similar to other experiments performed with epoxy encapsulants [3]. An LHS sensitivity analysis was performed using the time required for the bottom of the embedded component to reach 500 K. Only the thermal conductivity of the condensed phenolic was shown to correlate significantly with the response time. The other 20 parameters with uncertainty listed in Tables 1 and 2 do not have significant correlation with the response.

The "no strain" assumption in the MXB-71 constitutive model implies that there is no significant change in geometry of the phenolic during decomposition. This is not true above 900 °C as shown by vitrification of LFD samples prepared by curing 1-mm thick samples for 30 min at 925 °C in an oven. If there is significant strain, such as above 900 °C, the decomposition constitutive model should be coupled to a mechanical stress–strain constitutive model to account for the volume changes. Furthermore, the response of MXB-71 described in the current article does not depend on pressure. However, the prediction of pressure is possible using a low Mach flow assumption. Nevertheless, complete validation of the MXB-71 response model for hermetically sealed devices is not possible without more experiments. More work is also needed for radiation slip near shiny boundaries where the isotropic radiation diffusion approximation is not valid.

Acknowledgements Work performed at Sandia National Laboratories (SNL). Sandia is a multiprogram laboratory operated by Sandia Corporation, a Lockheed Martin Company, for the United States Department of Energy's National Nuclear Security Administration under Contract DE-AC04-94AL85000. We thank Ken Erickson, Walter Gill, John Oelfke, and Jill Suo-Anttila at SNL who contributed some of the data shown in this article. We would also like to thank the internal reviewers Tre' Shelton and Amanda B. Dodd. Comments and suggestions from external reviewers are also appreciated.

References

1. Hobbs ML, Erickson KL, Chu TY. Modeling decomposition of unconfined rigid polyurethane foam. Polym Degrad Stab. 2000;69:47–56.

2. Hobbs ML, Lemmon GH. Polyurethane foam response to fire in practical geometries. Poly Degrad Stab. 2004;84:183–97.
3. Hobbs ML. Modeling epoxy foams exposed to fire-like heat fluxes. Poly Degrad Stab. 2005;89:353–72.
4. Hobbs ML. Finite element modeling of syntactic foam. J Therm Anal Calorim 2006. doi:10.1007/s10973-005-7098-5.
5. Johnson RT Jr, Biefeld RM. Electrical conductivity changes associated with thermal decomposition of phenolic- and silicone-based materials. Polym Eng Sci. 1982;22:147–53.
6. Erickson KL. Thermal decomposition mechanisms common to polyurethane, epoxy, poly(diallyl phthalate), polycarbonate and poly (phenylene sulfide). J Therm Anal Calorim 2007. doi:10.1007/s10973-006-8218-6.
7. Chrissafis K. Kinetics of thermal degradation of polymers: complementary use of isoconversional and model-fitting methods. J Therm Anal Calorim 2009. doi:10.1007/s10973-008-9041-z.
8. McKay MD, Conover WJ, Beckman RJ. A comparison of three methods for selecting values of input variables in the analysis of output from a computer code. Technometrics. 1979;21:239–45.
9. Moghadassi AR, Hosseini SM, Henneke D, Elkamel A. A model of nanofluids effective thermal conductivity based on dimensionless groups. J Therm Anal Calorim 2009. doi:10.1007/s10973-008-9843-z.
10. Schuster J, Heider D, Sharp K. Measuring and modeling the thermal conductivities of three-dimensionally woven fabric composites. Mech Compos Mater. 2009;45:165–74.
11. Vozar L, Hohenauer W. Flash method of measuring the thermal diffusivity. A review. High Temp High Pres. 2004;35/36(3):253–64.
12. Pitt GJ. The kinetics of the evolution of volatile products from coal. Fuel. 1962;41:267–74.
13. Hobbs ML, Kaneshige MJ, Gilbert DW, Marley SK, Todd SN. Modeling TNT ignition. J Phys Chem A. 2009;113:10474–87.
14. Brill RB, Gongwer PE, Williams GK. Thermal decomposition of energetic materials. 66. Kinetic compensation effects in HMX, RDX, and NTO. J Phys Chem A. 1994;98:12242–7.
15. Hobbs ML, Romero VJ. Uncertainty analysis of decomposing polyurethane foam. Thermochim Acta. 2002;384:393–401.
16. Gibson LJ, Ashby MF. Cellular solids structure and properties. 2nd ed. Cambridge: Cambridge University Press; 1997.
17. Incropera FP, DeWitt DP. Fundamentals of heat and mass transfer. 5th ed. New York: Wiley; 2002.
18. Mottram JT, Geary B, Taylor R. Thermal expansion of phenolic resin and phenolic-fibre composites. J Mater Sci. 1992;27:5015–26.
19. Hobbs ML, Wente WB, Kaneshige MJ. PETN ignition experiments and models. J Phys Chem A. 2010;114:5306–19.
20. Siegel R, Howell JR. Thermal radiation heat transfer. 3rd ed. Washington, DC: Taylor & Francis; 1992.